

Article

A Fast Method for Uncertainty Analysis of Power System Dynamic Simulation

Chengxi Liu ^{1,2,*}, Youjin Jiang ^{1,2}, Hao Bai ³, Ruotian Yao ³, Lifang Wu ⁴ and Weichen Yang ³

¹ School of Electrical Engineering and Automation, Wuhan University, Wuhan 430072, China; 2017302540240@whu.edu.cn

² Hubei Engineering and Technology Research Center for AC/DC Intelligent Distribution Network, Wuhan 430072, China

³ Electric Power Research Institute of CSG, Guangzhou 510663, China

⁴ Electric Power Research Institute of Guangxi Power Grid, Nanning 530023, China

* Correspondence: liuchengxi@whu.edu.cn

Abstract: Uncertain variables, such as electric power system parameters, have significant impacts on dynamic simulations of power systems. As traditional uncertainty analysis methods for power system dynamic simulations, both the simulation method and the approximation methods are difficult to balance the model complexity, computational efficiency, and simulation accuracy. In order to balance the model complexity, computational efficiency, and simulation accuracy, this paper proposes a method for uncertainty analysis for power system dynamic simulation based on the Nataf transformation and Gaussian-Hermite quadrature. Firstly, the samples on the normal distribution space are determined according to the Gaussian-Hermite quadrature points and the Nataf transformation. Secondly, obtain the simulation samples by inverse Nataf transformation, and perform power system dynamic simulation. Thirdly, the random output is approximated as a linear combination of a single random input, and the mean and standard deviation of the random output under the impact of a single random input are calculated by Gaussian-Hermite quadrature. Then, calculate the mean and standard deviation of the random output under the impact of all random input. Finally, the effectiveness of the proposed method is validated on the IEEE 9-bus system and IEEE 39-bus system. Compared with Monte Carlo simulation and Latin Hypercube sampling, the proposed method can greatly reduce the simulation time for uncertain dynamic simulations while maintaining high accuracy.



Citation: Liu, C.; Jiang, Y.; Bai, H.; Yao, R.; Wu, L.; Yang, W. A Fast Method for Uncertainty Analysis of Power System Dynamic Simulation. *Processes* **2023**, *11*, 1886. <https://doi.org/10.3390/pr11071886>

Academic Editor: Hsin-Jang Shieh

Received: 25 April 2023

Revised: 19 June 2023

Accepted: 21 June 2023

Published: 23 June 2023



Copyright: © 2023 by the authors. Licensee MDPI, Basel, Switzerland. This article is an open access article distributed under the terms and conditions of the Creative Commons Attribution (CC BY) license (<https://creativecommons.org/licenses/by/4.0/>).

Keywords: uncertainty analysis; power system dynamic simulation; Nataf transformation; Gaussian-Hermite quadrature

1. Introduction

With the integration of a large number of new energy generation equipment and power electronic devices, the scale and complexity of modern power systems continue to expand. Large power grids with numerous devices, complex structures, and multiple time scales exhibit increasingly unpredictable dynamic behaviors, where local disturbances or faults can result in the oscillations, instability, or even collapse of the entire power grid. The complexity of modern power systems imposes higher requirements on the security and stability analysis of power systems, and improving the accuracy of dynamic models and parameters is of great significance. When a power outage occurred in the Western Interconnection of the United States, the dynamic simulation software of its power system could not obtain accurate results. Later analysis revealed that inaccurate load models might cause a large amount of error in the simulation results, fully demonstrating the importance of using correct load models and parameters for dynamic simulations of power systems [1,2]. As numerous renewable energy sources are connected to the power grid and the grid structure becomes more and more complex, the dynamic behavior of the power

system is affected by more and more uncertain factors, such as renewable energy outputs uncertainty, load power uncertainty, and parameter uncertainty. These uncertainties pose a severe challenge to the simulation of power system dynamic behavior. For example, when the output of the wind farm is a small value, the simulation results show that the power system is stable. However, due to the uncertainty of wind speed, the actual output of the wind farm is different from the value used in the simulation. The dynamic behavior of the system changes with the change in the actual output of the wind farm, and the stability of the system is a probability event.

However, most of the usual dynamic analysis uses deterministic theories and methods and rarely considers the influence of the uncertainty of the model, parameters, and renewable energy outputs on power system simulations.

Relevant works study the replacement of traditional analysis methods to achieve rapid and high-precision uncertainty analysis of power systems, mainly including interval analysis, serial operation theory, fuzzy theory [3], and credibility theory [4], which have been applied to power flow calculation, reliability assessment, power demand analysis, power quality assessment, and other aspects. In contrast, few researchers focus on the uncertainty analysis of power system dynamic simulation, mainly including sensitivity analysis [5], probability analysis [6,7], and interval analysis. Among them, probability analysis has been widely used in uncertainty analysis of power system dynamic simulation. At present, probability analysis methods for uncertainty analysis of power system dynamic simulation are mainly divided into two categories: simulation methods and approximation methods. As a simulation method, Monte Carlo simulation (MCS) is the most direct and effective probabilistic analysis method, when the sample size of MCS is large enough, the results are generally considered accurate. However, MCS is computationally inefficient and is usually used as a reference to verify the accuracy of other methods. Many studies have developed a more effective sampling technique to generate low-bias samples to replace the pseudo-random samples of MCS in order to speed up convergence and shorten computation time, among which Latin hypercube sampling (LHS) is the most popular technique. Compared with MCS, the Latin hypercube sampling method improves the convergence rate and thus the computational efficiency through a hierarchical sampling of the sample space [8]. However, in order to achieve the desired accuracy, the number of samples required for LHS is usually still large, so the computational efficiency of LHS in complex power systems needs to be further improved. Among the approximation methods for power system uncertainty analysis, the method based on polynomial chaos is the most widely used. In [9], a method of power system uncertainty analysis based on generalized polynomial chaos is proposed, which is more efficient than the MCS method. However, this method is difficult to adapt to the complex equipment model of the power system, and it requires a special differential algebraic equation solver. Reference [10] proposes a method of power system uncertainty analysis based on the probabilistic collocation method, which is suitable for quantifying the uncertainty of complex power systems. In [11,12], a non-intrusive multi-element polynomial chaos method is used to solve the problem of power system dynamic simulations with long-term uncertainty. The methods proposed in [10–12] are suitable for quantifying the uncertainty of complex power systems, but they do not consider the correlation between input random variables, and these methods could reduce the precision if allocated points are improperly selected [9]. In the past few years, many researchers have extended the application scope of the polynomial chaos method in uncertainty analysis of power systems. In view of the unknown probability distribution of random input, a data-driven polynomial chaos method is proposed in [13,14]. The data-driven polynomial chaos method is efficient and useful, but References [13,14] do not consider the correlation between the input random variables. In the power system, the similar load power and the change of new energy power are often correlated, and ignoring the correlation between these input random variables will produce a large error. In order to deal with the correlation between random inputs, Reference [15] uses a whitening transformation to transform random input variables into independent random

variables, and analyzes the uncertainty of the power system based on the data-driven polynomial chaos method. In view of the unknown probability distribution of random input, Reference [16] uses kernel density estimation to obtain the probability distribution of random input and then uses the polynomial chaos method to analyze the uncertainty of the power system. It should be pointed out that the method suitable for quantifying the uncertainty of complex power systems needs to satisfy the following characteristics: (1) The method can handle the correlation of input random variables; (2) The method needs to be non-intrusive [17], in order to adapt to complex power system models and use fast dynamic simulation algorithms [18,19]; (3) The method of determining dynamic simulation samples must be definite, and the number of samples should be as small as possible. However, the methods proposed in [8–16] cannot simultaneously satisfy these three characteristics. For example, simulation methods such as MCS and LHS are not computationally efficient enough. The approximation methods represented by polynomial chaos methods will suffer from the curse of dimensionality, and some improved polynomial chaos methods have difficulties in dealing with the correlation of random variables.

In view of the areas to be improved in the above research, this paper aims to propose an effective uncertainty analysis method for power system dynamic simulation, which can simultaneously satisfy the above three characteristics. In this paper, a fast power system uncertainty simulation method based on Nataf transformation and Gauss-Hermite quadrature is proposed. The main contributions are summarized as follows:

- (1) The whitening transformation in [15] is easy to implement when dealing with random input method dependencies, but this method has a large error when the random input deviates from the normal distribution. At the same time, the random distribution of the output of wind farms in the power system does not follow the normal distribution. In order to deal with the correlation between input random variables more accurately, this paper uses Nataf transformation to transform the original input random variable into independent standard normal random variables.
- (2) The objective of uncertainty analysis for power system dynamic simulation is to calculate the mean and standard deviation of random output variables on each time step, which is essentially a high-dimensional integral problem. Simulation methods such as MCS and LHS usually have high accuracy, but they are not computationally efficient enough. Simulation methods determine samples by random sampling, and the weights corresponding to all samples are the same and calculate the mean and standard deviation of output random variables according to the sample results. In fact, the selection of appropriate samples and weights based on the distribution of random inputs can greatly improve the speed of convergence and thus improve computational efficiency. Nataf transformation can be used to transform the problem into normal space, where Gauss Hermite quadrature has the highest precision. In order to improve computational efficiency, this paper proposes a fast power system uncertainty simulation method based on the Nataf transformation and Gauss-Hermite quadrature. Similar to the simulation methods, the method used in this paper is based on samples, so it is a non-intrusive method and can be applied to complex power systems.
- (3) Similar to the polynomial chaos methods, Gauss-Hermite quadrature also suffers from the curse of dimensionality. In order to reduce the impact of the curse of dimensionality, this paper approximates the high-dimensional objective function as a linear combination of one-dimensional functions, uses Gauss-Hermite quadrature to calculate the mean and standard deviation of one-dimensional functions, and finally calculates the mean and standard deviation of high-dimensional objective functions according to the mean and standard deviation of one-dimensional functions.

2. Uncertainty Analysis of Power System Dynamic Simulation Based on Nataf Transformation and Gauss-Hermite Quadrature

This section introduces the application of Nataf transformation and Gauss-Hermite quadrature to uncertainty analysis of power system dynamic simulations. Firstly, the process of converting the input random variable into an independent standard normal random variable by Nataf transformation is introduced. Then, this section introduces the method of determining the sample in the standard normal space and finally introduces the process of calculating the mean value and standard deviation of the output random variable based on the Gauss-Hermite quadrature.

2.1. Nataf Transformation

Under reasonable operating conditions, the random distribution of wind farm output usually follows the Weibull distribution, which makes the whitening transformation in [15] not applicable to the uncertainty analysis of power system dynamic simulation. To more accurately handle correlations between random inputs, the Morgenstern transformation, Rosenblatt transformation and Nataf transformation [20,21] can all be adopted. The Morgenstern transformation and Rosenblatt transformation require the joint distribution function of the random input variables, while the Nataf transform requires only the marginal distribution function of the random input variables. In power systems, there are often only marginal distribution functions and correlation coefficients of random variables. In this case, it is not feasible to use the Morgenstern transformation and Rosenblatt transformation for power system uncertainty analysis. In this section, the correlation of input random variables will be processed based on the Nataf transformation.

Suppose $\mathbf{X} = [x_1, x_2, \dots, x_d]^T$ is the d -dimensional random variable, $F_i(x_i)$ is the cumulative probability distribution function corresponding to the random variable, and the correlation coefficient matrix of the d -dimensional random variable is denoted by \mathbf{C}_X as

$$\mathbf{C}_X = \begin{bmatrix} 1 & \rho_{12} & \cdots & \rho_{1d} \\ \rho_{21} & 1 & \cdots & \rho_{2d} \\ \vdots & \vdots & \ddots & \vdots \\ \rho_{d1} & \rho_{d2} & \cdots & 1 \end{bmatrix} \quad (1)$$

Through the edge transformation corresponding to Equation (2), \mathbf{X} can be transformed into a set of standard normally distributed random variables which is denoted as $\mathbf{Y} = [y_1, y_2, \dots, y_d]^T$

$$y_k = \Phi^{-1}(F_k(x_k)), k = 1, 2, \dots, d \quad (2)$$

Φ is the cumulative probability distribution function corresponding to the standard normal distribution, and Φ^{-1} is its inverse function. The correlation coefficient matrix of \mathbf{Y} is denoted by \mathbf{C}_Y as

$$\mathbf{C}_Y = \begin{bmatrix} 1 & \rho'_{12} & \cdots & \rho'_{1d} \\ \rho'_{21} & 1 & \cdots & \rho'_{2d} \\ \vdots & \vdots & \ddots & \vdots \\ \rho'_{d1} & \rho'_{d2} & \cdots & 1 \end{bmatrix} \quad (3)$$

For the above transformation, the corresponding elements of \mathbf{C}_X and \mathbf{C}_Y satisfy the relation shown in Equation (4).

$$\rho_{ij} = \int_{-\infty}^{+\infty} \int_{-\infty}^{+\infty} \left(\frac{x_i - \mu_i}{\delta_i} \right) \left(\frac{x_j - \mu_j}{\delta_j} \right) \varphi_2(y_i, y_j, \rho'_{ij}) dy_i dy_j \quad (i \neq j) \quad (4)$$

In the above equations, μ_i and μ_j are the mean values of the random variables x_i, x_j , δ_i and δ_j are their corresponding standard deviations. \mathbf{Y} is a set of standard, normally distributed random variables with correlation coefficient matrix \mathbf{C}_Y , which can be transformed

into a set of independent standard normally distributed random variables by Cholesky decomposition.

Firstly, the Cholesky decomposition of C_Y is performed by Equation (5), which can be expressed as

$$LL^T = C_Y \tag{5}$$

Then, the independent standard normally distributed random variable $Z = [z_1, z_2, \dots, z_d]^T$ can be expressed as:

$$Z = L^{-1}Y \tag{6}$$

Equations (1)–(6) constitute the Nataf transformation process, while the inverse Nataf transformation is the process of solving X when Z is known, which can be expressed by Equation (7) as

$$Y = LZ, \\ x_i = F_i^{-1}(\Phi(y_i)), i = 1, 2, \dots, d \tag{7}$$

In Equation (7), F_i^{-1} is the inverse function of F_i .

Reference [22] puts forward an empirical formula for solving Equation (4), which can be expressed as

$$\rho'_{ij} = F\rho_{ij} \tag{8}$$

F is a function of $F_i(x_i)$, $F_j(x_j)$, and ρ_{ij} . For example, when x_i and x_j are both Weibull distributions for wind power [23], Equation (9) can be obtained, which can be expressed as

$$F = 1.063 - 0.04\rho_{ij} - 0.2\left(\frac{\delta_i}{\mu_i} + \frac{\delta_j}{\mu_j}\right) - 0.001\rho_{ij}^2 + \\ 0.337\left(\frac{\delta_i^2}{\mu_i^2} + \frac{\delta_j^2}{\mu_j^2}\right) + 0.007\rho_{ij}\left(\frac{\delta_i}{\mu_i} + \frac{\delta_j}{\mu_j}\right) - 0.007\frac{\delta_i\delta_j}{\mu_i\mu_j} \tag{9}$$

2.2. Uncertainty Analysis of Single Input Random Variable Based on Gauss-Hermite Quadrature

For a response function of one variable $S = S(x)$, the sampling points and weights are determined on the independent standard normal space according to the Hermite polynomials. The sampling points and weights can be obtained directly by table lookup, and the calculation time can be reduced without repeated calculation of sampling points. Table 1 shows the sampling points and the corresponding integral weights when there are 3, 5, and 7 sampling points. In Table 1 z^j is the j th sampling point, P is the sampling number and A_j is the corresponding weight of the j th sampling point.

Table 1. Partial Gaussian-Hermite quadrature points and corresponding integral weights.

P	z^j	A_j
3	± 1.7320508	0.16666667
	0	0.66666667
	± 2.85697001	0.01125741
5	± 1.35562618	0.22207592
	0	0.53333333
	± 3.75043972	0.00054827
7	± 2.36675941	0.03075712
	± 1.15440539	0.24012318
	0	0.45714286

If inverse Nataf transformation is denoted as N^{-1} , Equation (10) can be obtained as

$$S(x) = S(N^{-1}(z)) \tag{10}$$

In Equation (10), z represents the standard normal random variable. According to the Gauss-Hermite quadrature formula [24,25], the mean μ_S and standard deviation σ_S of the output random variable S can be obtained, as shown in Equation (11).

$$\begin{aligned}\mu_S &\approx \sum_{j=1}^P A_j S(N^{-1}(z_j)) \\ \sigma_S &\approx \sqrt{\sum_{j=1}^P A_j (S(N^{-1}(z_j)) - \mu_S)^2}\end{aligned}\quad (11)$$

2.3. Uncertainty Analysis of Multiple Input Random Variable Based on Gauss-Hermite Quadrature

When there is only one input random variable, Equation (11) can calculate the mean value and standard deviation of the output random variable. In practical applications, where the number of input random variables is usually greater than 1, the response function S is a function of the input random variables $\mathbf{X} = [x_1, x_2, \dots, x_d]^T$. In this case, the simplest and most accurate method is to take P sampling points for each variable, so P^d samples are needed for d input random variables. This method is simple to implement and can obtain accurate mean and standard deviation of output random variables. However, this method requires P^d calculations, and the calculation amount will show an exponential growth trend with the increase in the number of input random variables.

In order to reduce the number of calculations, this paper adopts the method proposed in [26] to approximate the target response function, which can be expressed by Equation (12) as

$$S_{\Sigma}(\mathbf{X}) \approx \sum_{i=1}^d (S_i(x_i) - S_{\Sigma}(\mathbf{X}_{\mu})) + S_{\Sigma}(\mathbf{X}_{\mu}) \quad (12)$$

In Equation (12), $S_{\Sigma}(\mathbf{X}_{\mu})$ represents the function value of the objective response function S_{Σ} when all input random variables are mean values. In practical engineering applications, $S_{\Sigma}(\mathbf{X}_{\mu})$ is the simulation value of the objective response function S_{Σ} when all input random variables are mean values. $S_i(x_i)$ is the univariate function of $S_{\Sigma}(\mathbf{X})$ with respect to x_i , and all the other input random variables are the mean values. The input random variables \mathbf{X} are transformed into a set of independent standard normal random variables \mathbf{Z} by Nataf transformation, then $S_i(x_i)$ can be expressed as

$$S_i(x_i) = S_i(N^{-1}(z_i)) \quad (13)$$

Through Equation (11), the mean μ_{S_i} and standard deviation σ_{S_i} of $S_i(x_i)$ can be expressed as

$$\begin{aligned}\mu_{S_i} &\approx \sum_{j=1}^P A_j S_i(N^{-1}(z_i^j)) \\ \sigma_{S_i} &\approx \sqrt{\sum_{j=1}^P A_j (S_i(N^{-1}(z_i^j)) - \mu_{S_i})^2}\end{aligned}\quad (14)$$

After obtaining the mean μ_{S_i} and standard deviation σ_{S_i} of $S_i(x_i)$, the mean $\mu_{S_{\Sigma}}$ and standard deviation $\sigma_{S_{\Sigma}}$ of the target response function S_{Σ} can be expressed as

$$\begin{aligned}\mu_{S_{\Sigma}} &\approx \sum_{i=1}^d (\mu_{S_i} - S_{\Sigma}(\mathbf{X}_{\mu})) + S_{\Sigma}(\mathbf{X}_{\mu}) \\ \sigma_{S_{\Sigma}} &\approx \sqrt{\sum_{i=1}^d \sigma_{S_i}^2}\end{aligned}\quad (15)$$

This method requires that the computation times of the objective response function S_{Σ} are $(P - 1)d + 1$ and that the computation times of the objective response function increase linearly with the number of input random variables d and the number of sampling points P .

2.4. Uncertainty Analysis of Power System Dynamic Simulation Based on Gauss-Hermite Quadrature

The essence of dynamic simulations of power systems is to solve a set of nonlinear differential-algebraic equations (DAEs) [27]. DAEs of the power system can be expressed as

$$\begin{aligned} \frac{d\zeta}{dt} &= f(\zeta, \tau) \\ 0 &= g(\zeta, \tau) \end{aligned} \quad (16)$$

In Equation (16), ζ represents the state variables vector of the power system, such as generator power angle, generator speed, excitation voltage of the exciter, and output power of the turbine. τ represents the algebraic variables vector of the power system, such as voltage amplitude, voltage phase angle, and the current of each device. f and g are nonlinear function vectors of ζ and τ . When there are uncertain parameters in the power system, the DAEs are expressed as

$$\begin{aligned} \frac{d\zeta}{dt} &= f(\zeta, \tau, \mathbf{X}) \\ 0 &= g(\zeta, \tau, \mathbf{X}) \end{aligned} \quad (17)$$

In Equation (17), \mathbf{X} are the input random variables. This paper considers the randomness of wind farm output and load power. Wind speed varies with time and place, and its probability density function (PDF) is claimed to be Weibull. Therefore, wind speed is modeled using the Weibull distribution function. In the linear operation region, the PDF of wind farm output can be expressed as

$$PDF(P_w) = \frac{\beta}{\eta^\beta} (P_w)^{\beta-1} \exp\left(-\left(\frac{P_w}{\eta}\right)^\beta\right) \quad (18)$$

In Equation (18), P_w is the wind farm output, β is the shape parameter and η is the scale parameter. The load power is usually modeled as the normal distribution.

Considering the input random variables \mathbf{X} , the following relation can be obtained as

$$\begin{aligned} \zeta_t &= F_t(\mathbf{X}), \zeta \in \zeta \\ \tau_t &= G_t(\mathbf{X}), \tau \in \tau \end{aligned} \quad (19)$$

In Equation (19), ζ_t and τ_t are the values of ζ and τ at time t , respectively. F_t and G_t are target response functions similar to S_Σ in Equation (12), so the mean and standard deviation of ζ_t and τ_t can be obtained by Equations (12)–(15).

The detailed steps of uncertainty analysis for dynamic simulation of power system based on Gauss-Hermite quadrature are shown in Figure 1 and the general steps are as follows

- (1) Input the correlation coefficient matrix C_X , the number of random input variables d , and the number of Gauss-Hermite quadrature points P .
- (2) Calculate matrix C_Y by Equation (4), and calculate matrix L by Equation (5).
- (3) Based on the Gauss-Hermite quadrature points and weight listed in Table 1, determine the samples corresponding to \mathbf{Z} in the normal space.
- (4) Based on the samples corresponding to \mathbf{Z} , determine the samples corresponding to the input random variables \mathbf{X} by Equation (7).
- (5) Solve Equation (17) according to each sample in \mathbf{X} , and obtain the values of ζ and τ at time t .
- (6) Calculate the mean and standard deviation of each random variable x_i in \mathbf{X} according to Equations (13) and (14).
- (7) Calculate the mean and standard deviation of the response function of multiple random variables \mathbf{X} by Equation (15).

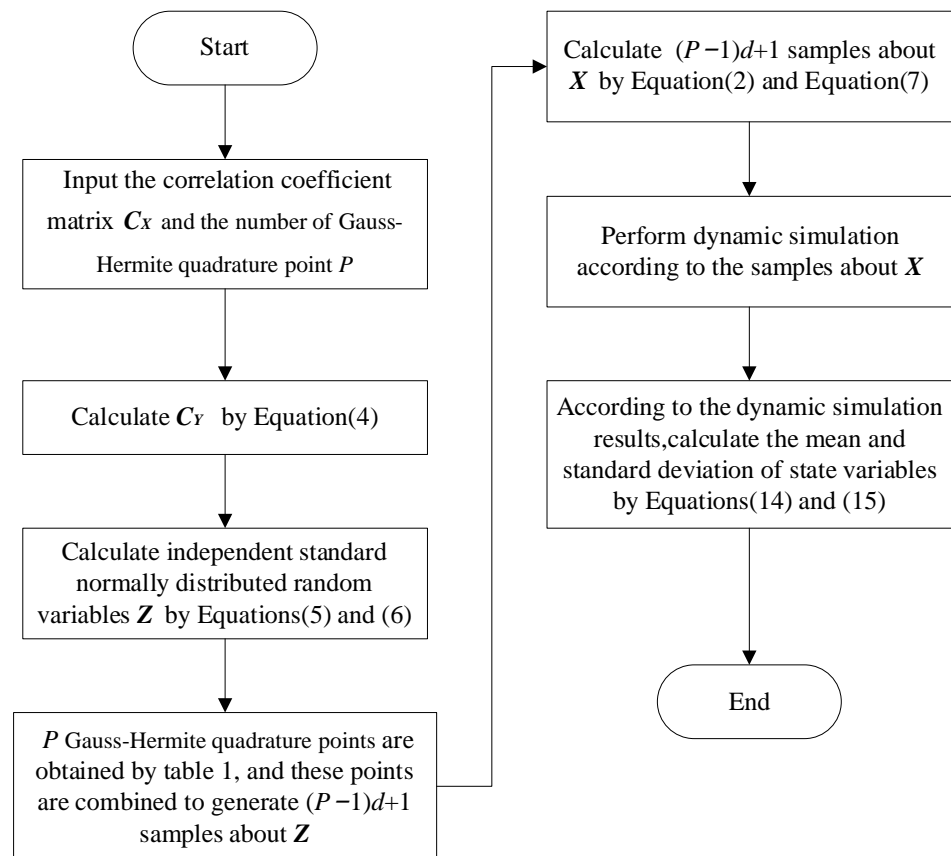


Figure 1. The detailed steps of the proposed method.

3. Case Studies

The IEEE 9—bus system and IEEE 39—bus system are used for the case study. The simulation is performed in MATLAB 2021a on a personal computer with a 2.9 GHz i5 processor and 16 GB RAM. Regarding random input variables, this paper considers the influence of the randomness of wind farm output and load power on power system dynamic simulation. Power angle stability, frequency stability, and voltage stability are the three important parts of power system stability analysis, so this paper analyzes the influence of random input on power system dynamic simulation from the perspectives of rotation angle, rotation speed, and voltage amplitude. When the sample size of MCS is large enough, the method will converge to an exact value, so this paper uses the mean and standard deviation of the random output calculated by convergent MCS as the standard values. To verify the accuracy of the proposed method, the mean and standard deviation calculated by the proposed method are compared with the standard values. Furthermore, the proposed method will be compared with LHS for the purpose of comparing the accuracy and computational efficiency of the two methods.

3.1. Case study of the IEEE 9-Bus System

3.1.1. Simulation Setup Description

The topology of the IEEE 9—bus system is illustrated in Figure 2. Partial static parameters for the IEEE 9—bus system can be found in Table A1. Other static parameters can be found in [28]. Synchronous generators adopt the classical model and loads adopt the constant impedance model. For the bus with a generator and the bus without a generator, the dynamic model adopted can be expressed as Equations (20) and (21), respectively.

$$\begin{aligned}
\frac{d\delta_i}{dt} &= \omega_s \omega_i \\
\frac{d\omega_i}{dt} &= \frac{1}{2H} (P_{mi} - P_{ei} - D_i \omega_i) \\
P_{ei} &= V_{di} I_{di} + V_{qi} I_{qi} + (I_{di}^2 + I_{qi}^2) R_{ai} \\
\begin{bmatrix} \sin \delta_i & \cos \delta_i \\ -\cos \delta_i & \sin \delta_i \end{bmatrix} \begin{bmatrix} I_{di} \\ I_{qi} \end{bmatrix} &= \frac{1}{R_{ai}^2 + X'_{di}{}^2} \begin{bmatrix} R_{ai} & X'_{di} \\ -X'_{di} & R_{ai} \end{bmatrix} \begin{bmatrix} E'_{qi} \cos \delta_i - \sin \delta_i V_{di} - \cos \delta_i V_{qi} \\ E'_{qi} \sin \delta_i + \cos \delta_i V_{di} - \sin \delta_i V_{qi} \end{bmatrix} \\
0 &= (V_{di} I_{di} + V_{qi} I_{qi}) - P_{Li} - V_{mi} \sum_{j=1}^{nb} V_{mj} (G_{ij} \cos \theta_{ij} + B_{ij} \sin \theta_{ij}) \\
0 &= (-V_{di} I_{qi} + V_{qi} I_{di}) - Q_{Li} - V_{mi} \sum_{j=1}^{nb} V_{mj} (G_{ij} \sin \theta_{ij} - B_{ij} \cos \theta_{ij}) \\
P_{Li} &= P_{Li0} \left(\frac{V_{mi}}{V_{mi0}} \right)^2, Q_{Li} = Q_{Li0} \left(\frac{V_{mi}}{V_{mi0}} \right)^2, \theta_{ij} = \theta_i - \theta_i, V_{di} + jV_{qi} = V_{mi} (\cos \theta_i + j \sin \theta_i) e^{-j(\delta_i - \pi/2)} \\
i &\in \mathbf{G}
\end{aligned} \tag{20}$$

$$\begin{aligned}
0 &= -P_{Li} - V_{mi} \sum_{j=1}^{nb} V_{mj} (G_{ij} \cos \theta_{ij} + B_{ij} \sin \theta_{ij}) \\
0 &= -Q_{Li} - V_{mi} \sum_{j=1}^{nb} V_{mj} (G_{ij} \sin \theta_{ij} - B_{ij} \cos \theta_{ij}) \\
P_{Li} &= P_{Li0} \left(\frac{V_{mi}}{V_{mi0}} \right)^2, Q_{Li} = Q_{Li0} \left(\frac{V_{mi}}{V_{mi0}} \right)^2, \theta_{ij} = \theta_i - \theta_i \\
i &\in \mathbf{NG}
\end{aligned} \tag{21}$$

where δ_i and ω_i are state variables, representing the rotation angle and rotation speed deviations of generator i ; V_{di} , V_{qi} , I_{di} , I_{qi} , and P_{ei} are d - and q -axes voltages and currents and the electrical power; V_{mi} and θ_i are the voltage amplitude and voltage phase angle; \mathbf{G} and \mathbf{NG} denote the sets of a bus with generator and bus without generator respectively, and nb represents the number of buses. P_{Li0} and Q_{Li0} are the initial active power and initial reactive power of the load. P_{mi} and E'_{qi} are the mechanical power and q -axes transient field voltages of generator i . The initial values of variables satisfy Equation (22), where P_{Gi} and Q_{Gi} are the active power and reactive power of the generator, and the subscript 0 represents the initial value of the variable. All others are parameters, details can be found in Tables A2 and A3.

$$\begin{aligned}
&\text{for } i \in \mathbf{G}, \theta_{ij0} = \theta_{i0} - \theta_{i0} \\
0 &= P_{Gi} - P_{Li0} - V_{mi0} \sum_{j=1}^{nb} V_{mj0} (G_{ij} \cos \theta_{ij0} + B_{ij} \sin \theta_{ij0}) \\
0 &= Q_{Gi} - Q_{Li0} - V_{mi0} \sum_{j=1}^{nb} V_{mj0} (G_{ij} \sin \theta_{ij0} - B_{ij} \cos \theta_{ij0}) \\
P_{mi0} &= P_{ei0}, \omega_{i0} = 0 \\
E_{Qi} &= V_{mi0} (\cos \theta_{i0} + j \sin \theta_{i0}) + (R_{ai} + jX'_{di}) \frac{P_{Gi} - jQ_{Gi}}{V_{mi0} (\cos \theta_{i0} + j \sin \theta_{i0})} \\
\delta_{i0} &= \text{angle}(E_{Qi}), E'_{qi} = \text{abs}(E_{Qi}) \\
&\text{for } i \in \mathbf{NG}, \theta_{ij0} = \theta_{i0} - \theta_{i0} \\
0 &= -P_{Li0} - V_{mi0} \sum_{j=1}^{nb} V_{mj0} (G_{ij} \cos \theta_{ij0} + B_{ij} \sin \theta_{ij0}) \\
0 &= -Q_{Li0} - V_{mi0} \sum_{j=1}^{nb} V_{mj0} (G_{ij} \sin \theta_{ij0} - B_{ij} \cos \theta_{ij0})
\end{aligned} \tag{22}$$

In this case, P_{G2} and P_{G3} are the random inputs of interest. P_{G2} and P_{G3} are subject to two-parameter Weibull distribution, which is measured in megawatts, the scale parameters are 30, and the shape parameters are 4. The correlation coefficient between the active power output of G2 and G3 is 1/10. The simulation time step is 1 millisecond, and the total simulation time is 5 s. At 0.9 s, a three-phase gold short circuit occurs in bus 8, and the fault is cleared at 1 s by cutting outlines 8–9. The Monte Carlo simulation method (MCS) of 10,000 times is used as the comparison standard. The method proposed in this paper is

denoted as NGHQ. The NGHQ is compared with MCS and the Latin hypercube sampling (LHS) in [29]. P is the number of samples, and the results of three different P are analyzed.

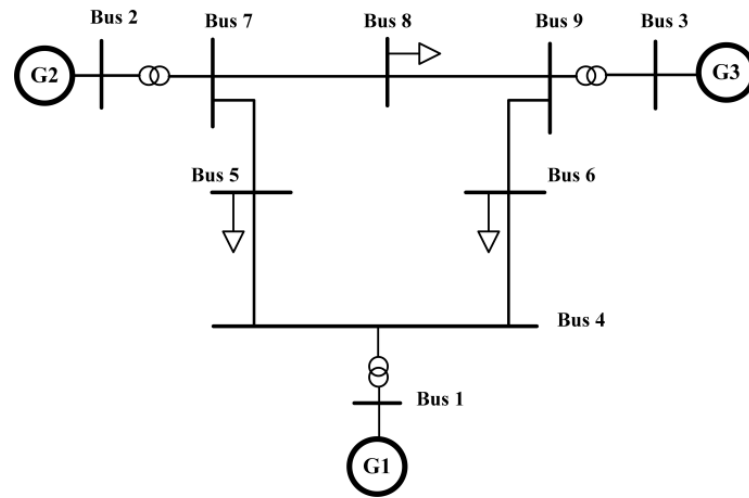


Figure 2. Topology of the IEEE 9—bus system.

3.1.2. Simulation Results Analysis

The relative rotation angle of generator 1 and generator 2 is denoted as δ_{21} . Figure 3 shows the mean value of δ_{21} calculated by three different methods when the P value of NGHQ is 5. Figure 4 shows the standard deviation of δ_{21} calculated by three different methods. The relative variation of the rotation speed of generator 1 and generator 2 is denoted as ω_{21} . Figure 5 shows the mean value of ω_{21} calculated by three different methods. Figure 6 shows the standard deviation of ω_{21} calculated by three different methods. From Figures 2–5, it can be seen that the mean values of state variables calculated by method NGHQ have little difference with MCS and LHS. In addition, the accuracy of the standard deviations of the state variables calculated by NGHQ and LHS are slightly lower than that of MCS, and the errors of NGHQ and LHS accumulate over the simulation time. At the same time, the accuracy of LHS (1000 times) is slightly higher than that of NGHQ ($P = 5$). It should be pointed out that the accuracy of standard deviation obtained by method NGHQ and LHS are satisfactory for practical engineering applications over a long period of time.

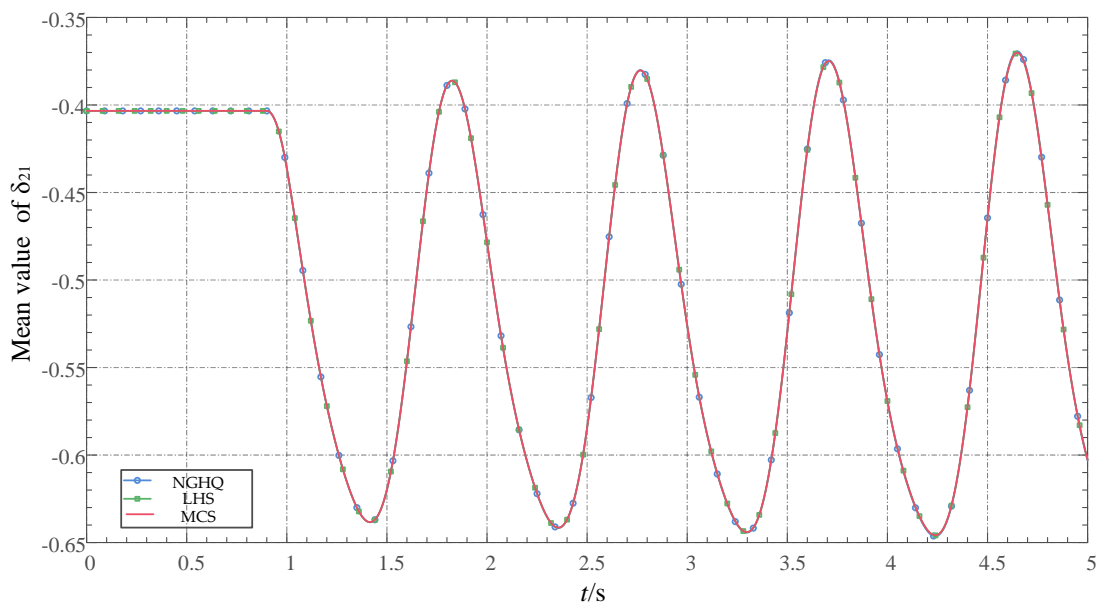


Figure 3. The mean values of δ_{21} about three different methods in the IEEE 9—bus system.

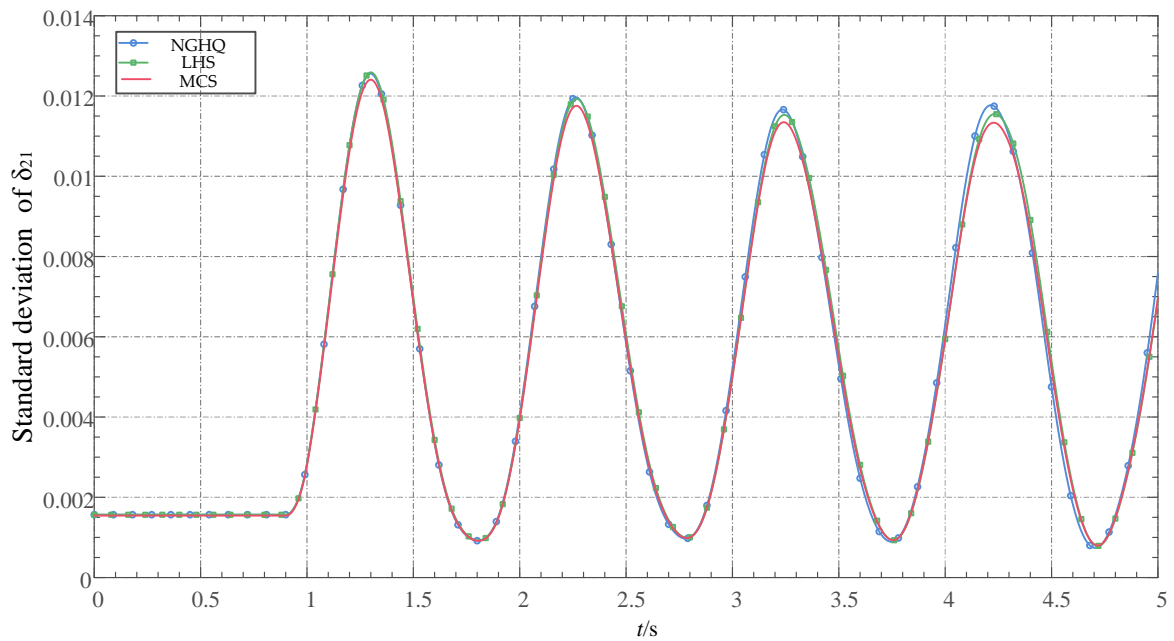


Figure 4. The standard deviations of δ_{21} about three different methods in the IEEE 9—bus system.

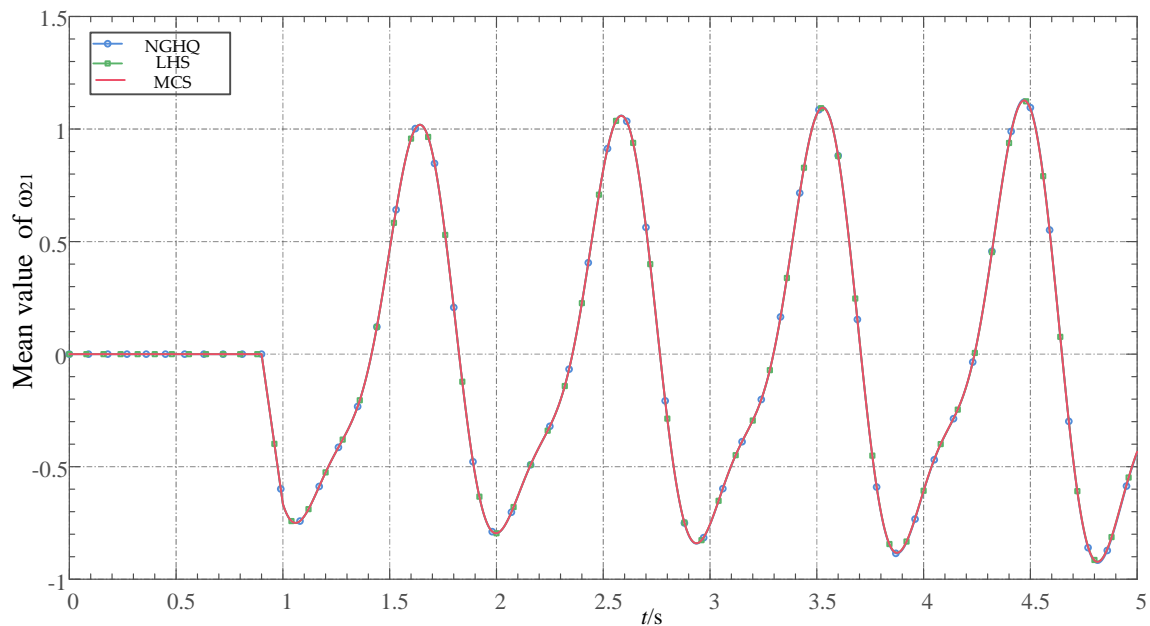


Figure 5. The mean values of ω_{21} about three different methods in the IEEE 9—bus system.

The voltage amplitude of bus 5 is denoted as V_{m5} . Figure 7 shows the mean value of V_{m5} calculated by three different methods when the P -value of NGHQ is 5. Figure 8 shows the standard deviation of V_{m5} calculated by three different methods. From Figures 7 and 8, it can be seen that the mean values and standard deviation of algebraic variables calculated by method NGHQ have little difference with LHS. The mean values of NGHQ and LHS are very close to that of MCS, but the standard deviations of these two methods have an acceptable error. To more intuitively compare the accuracy of the proposed method and LHS, Table 2 shows the mean values and standard deviations of each voltage amplitude at 1 s. As can be seen from Table 2, the mean values calculated by the three methods are the same, while the accuracy of LHS is slightly higher than that of NGHQ in terms of standard deviations. In practice, the accuracy of both LHS and NGHQ is acceptable, but the computational efficiency of NGHQ is much higher than that of LHS.

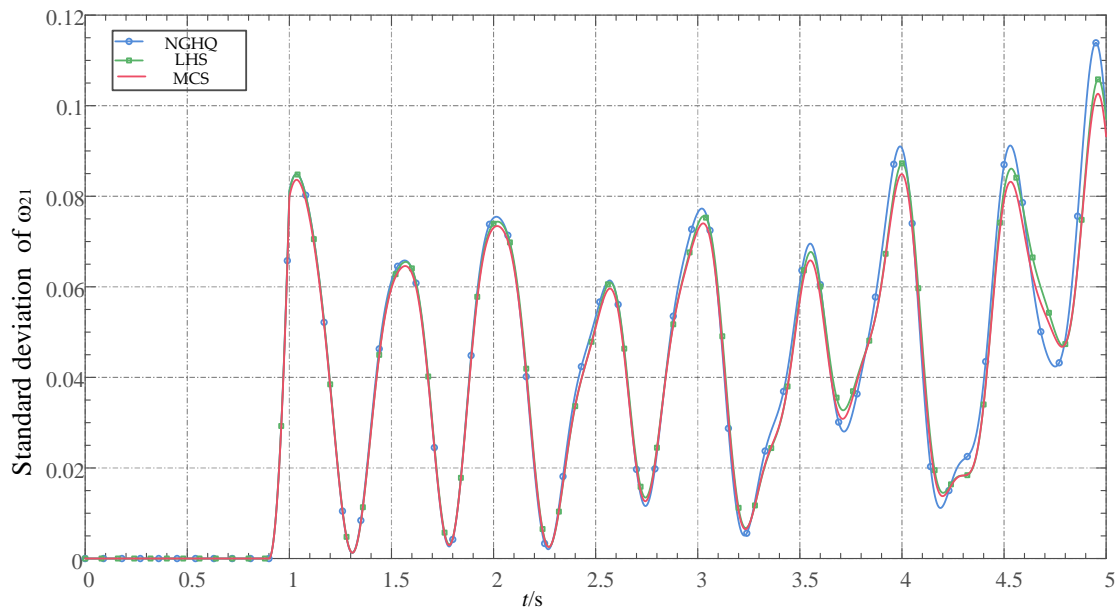


Figure 6. The standard deviations of ω_{21} about three different methods in the IEEE 9—bus system.

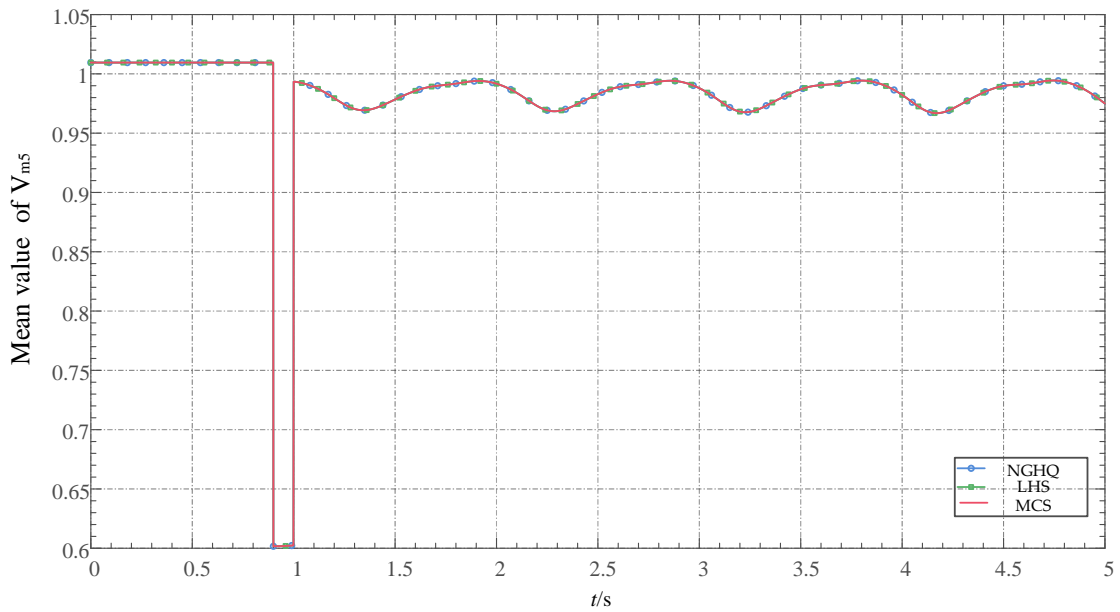


Figure 7. The mean values of V_{m5} about three different methods in the IEEE 9—bus system.

Table 2. Mean values and standard deviations of each voltage amplitude of different methods at 1 s.

	Mean Values/pu			Standard Deviations/pu		
	MCS	LHS	NGHQ	MCS	LHS	NGHQ
V_{m1}	1.0326	1.0326	1.0326	3.5476×10^{-7}	3.5917×10^{-7}	3.6209×10^{-7}
V_{m2}	1.0234	1.0234	1.0234	2.3199×10^{-7}	2.3801×10^{-7}	2.1877×10^{-7}
V_{m3}	1.0180	1.0180	1.0180	3.0728×10^{-7}	3.1996×10^{-7}	3.4154×10^{-7}
V_{m4}	1.0052	1.0052	1.0052	7.9225×10^{-7}	8.1212×10^{-7}	8.0810×10^{-7}
V_{m5}	0.9935	0.9935	0.9935	4.1470×10^{-6}	4.2455×10^{-6}	4.2142×10^{-6}
V_{m6}	1.0175	1.0175	1.0175	2.5313×10^{-6}	2.5851×10^{-6}	2.6270×10^{-6}
V_{m7}	1.0051	1.0051	1.0051	1.0861×10^{-6}	1.1121×10^{-6}	1.1459×10^{-6}
V_{m8}	1.0184	1.0184	1.0184	3.0746×10^{-7}	3.1716×10^{-7}	3.2355×10^{-7}
V_{m9}	0.9546	0.9546	0.9546	1.0169×10^{-6}	1.0425×10^{-6}	1.0332×10^{-6}

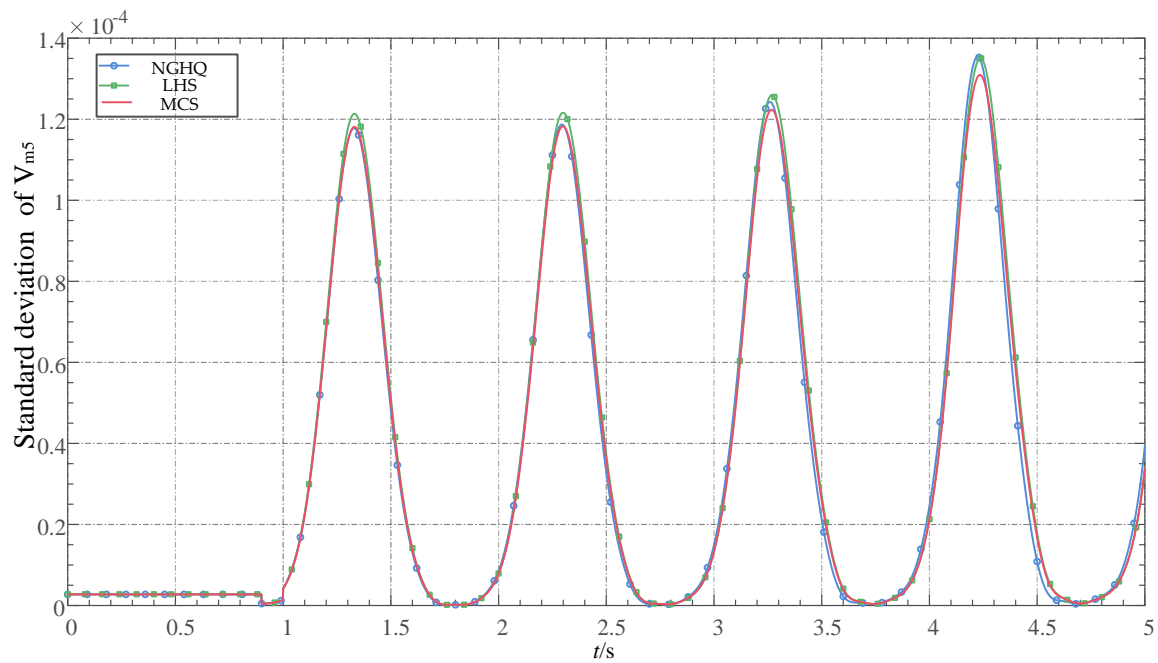


Figure 8. The standard deviations of V_{m5} about three different methods in the IEEE 9—bus system.

At the same time, it can be seen from the results of Figures 9 and 10 that there is no significant difference in the results obtained by method NGHQ under different P . The errors of method NGHQ are mainly derived from Equations (11) and (12), and different P only affect the errors of Equation (11). That is to say, in this example, when $P = 3$, the error of Equation (11) already meets the requirements, and increasing the number of sampling points will have little impact on the accuracy. Table 3 shows the number of deterministic dynamic simulations N and the total calculation time T in various scenarios. As can be seen from Table 3, compared to MCS and LHS, the proposed method can reduce a large number of dynamic simulation times, thus greatly improving the computational efficiency.

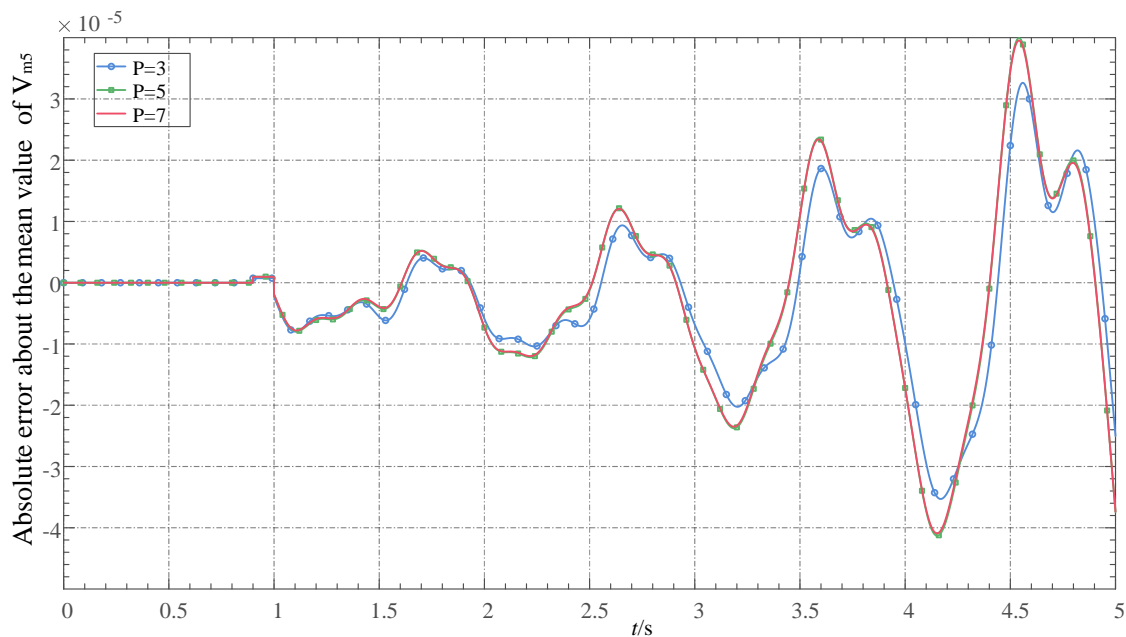


Figure 9. The absolute error about mean values of V_{m5} about three different P in the IEEE 9—bus system.

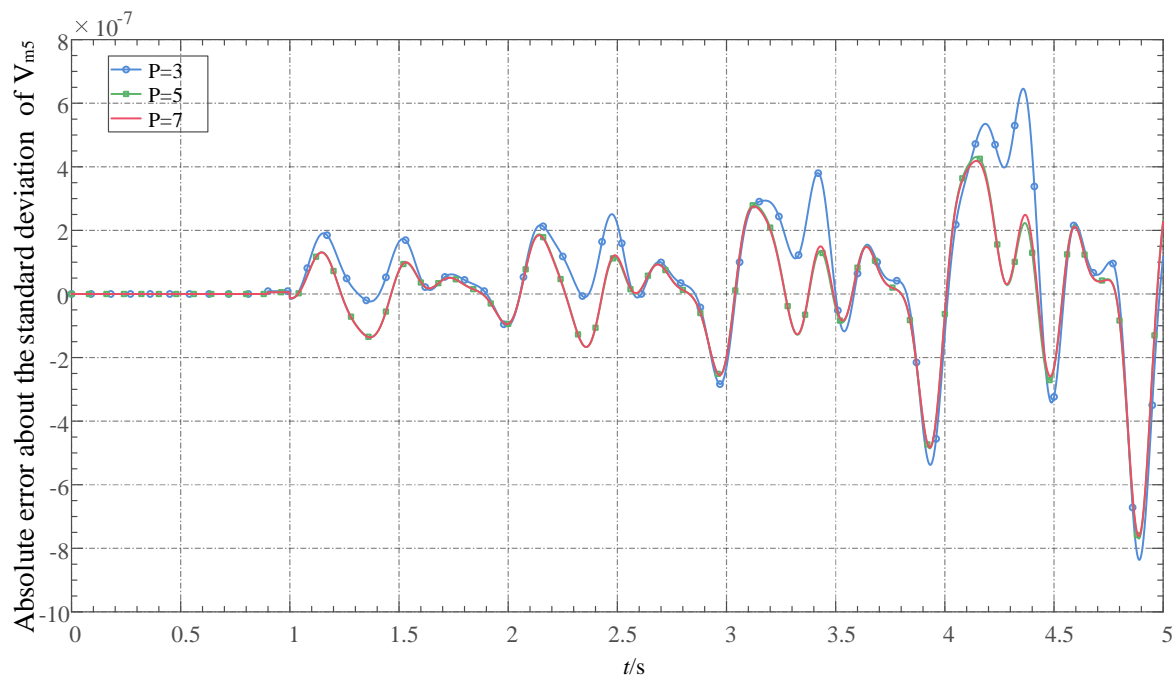


Figure 10. The absolute error about standard deviations of V_{m5} about three different P in the IEEE 9—bus system.

Table 3. Simulation times and calculation time of different scenarios in the IEEE 9—bus system.

Scenarios	N	T/s
MCS	10,000	9610.25
NGHQ — $P = 3$	5	4.93
NGHQ — $P = 5$	9	8.71
NGHQ — $P = 7$	13	12.34
LHS	1000	963.42

3.2. Case Study of the IEEE 39-Bus System

3.2.1. Simulation Setup Description

The description of the IEEE 39—bus system can be found in [30] and the static parameters can be found in [28]. A 6th-order generator model, a 1st-order exciter, a 1st-order governor, and the load model with ZIP are adopted for the IEEE 39—bus system. The percentages of constant-impedance, constant-current, and constant-power components of all loads are 70%, 10%, and 20%. The dynamic model used in this case is similar to that used in the IEEE 9—bus system, except that the generator model is more complex, so the model will not be described here. The detailed equations of the dynamic model can be found in [31]. The dynamic parameters used in this paper are the same as those in [18,31]. In this case study, the initial values of P_{L1} and P_{L18} are the random inputs of interest, and it is assumed that active power in Load 1 follows the Gaussian distribution with the mean being the original load active power and the standard deviation being 5%. The active power in Load 18 also follows the Gaussian distribution with the mean being the original load active power and the standard deviation being 5%. The correlation coefficient between the active power of Load 1 and Load 18 is 1/2. The simulation time step is 1 millisecond, and the total simulation time is 5 s. At 1 s, a three-phase line break occurs on lines 8–9. The NGHQ, which 5 quadrature points are used for, is compared with MCS of 20,000 times simulation and LHS of 1000 times simulation.

3.2.2. Simulation Results Analysis

The rotor angle of Generator 2 with respect to that of Generator 1, δ_{21} , and its relative rotation speed variation, ω_{21} , are selected to analyze the results. Figure 11 shows the mean value of δ_{21} calculated by three different methods. Figure 12 shows the standard deviation of δ_{21} calculated by three different methods. Figure 13 shows the mean value of ω_{21} calculated by three different methods. Figure 14 shows the standard deviation of ω_{21} calculated by three different methods.

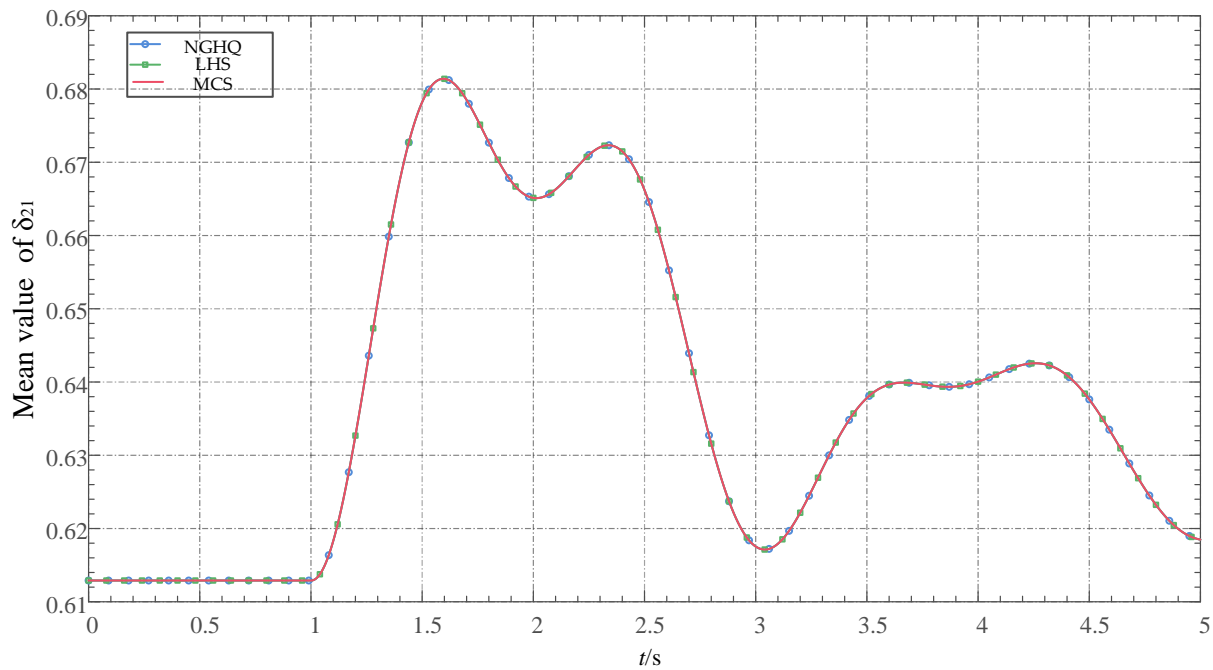


Figure 11. The mean values of δ_{21} about three different methods in the IEEE 39—bus system.

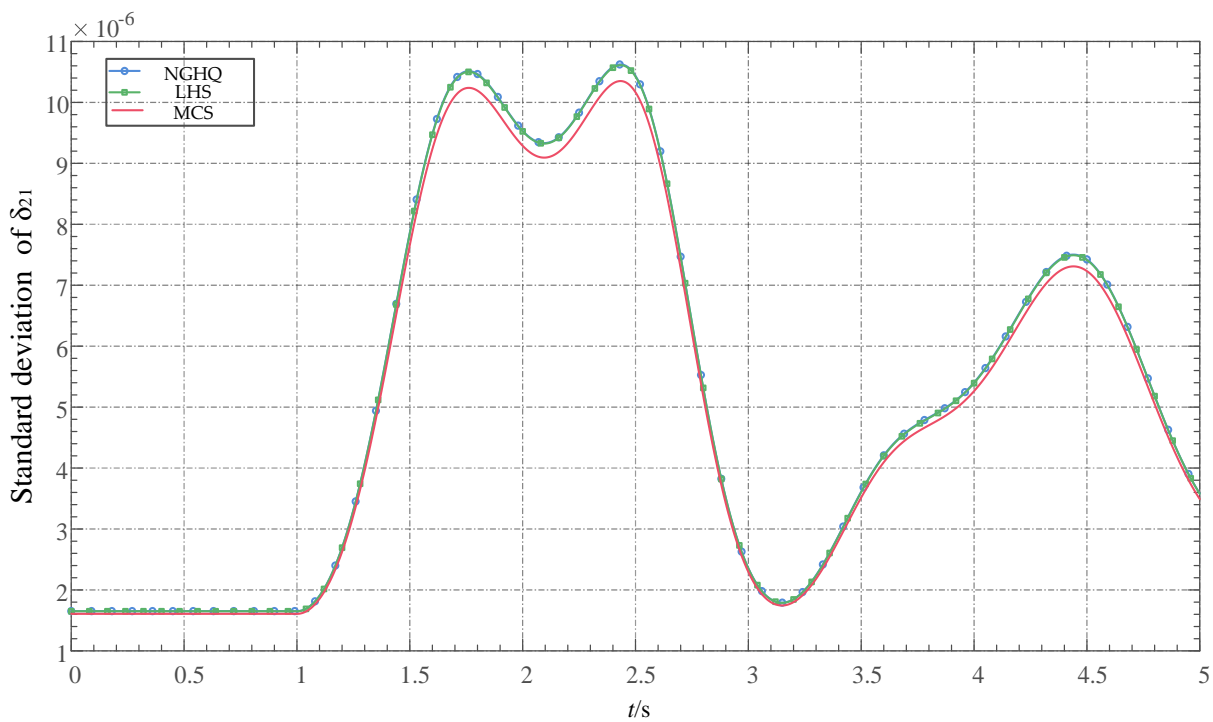


Figure 12. The standard deviations of δ_{21} about three different methods in the IEEE 39—bus system.

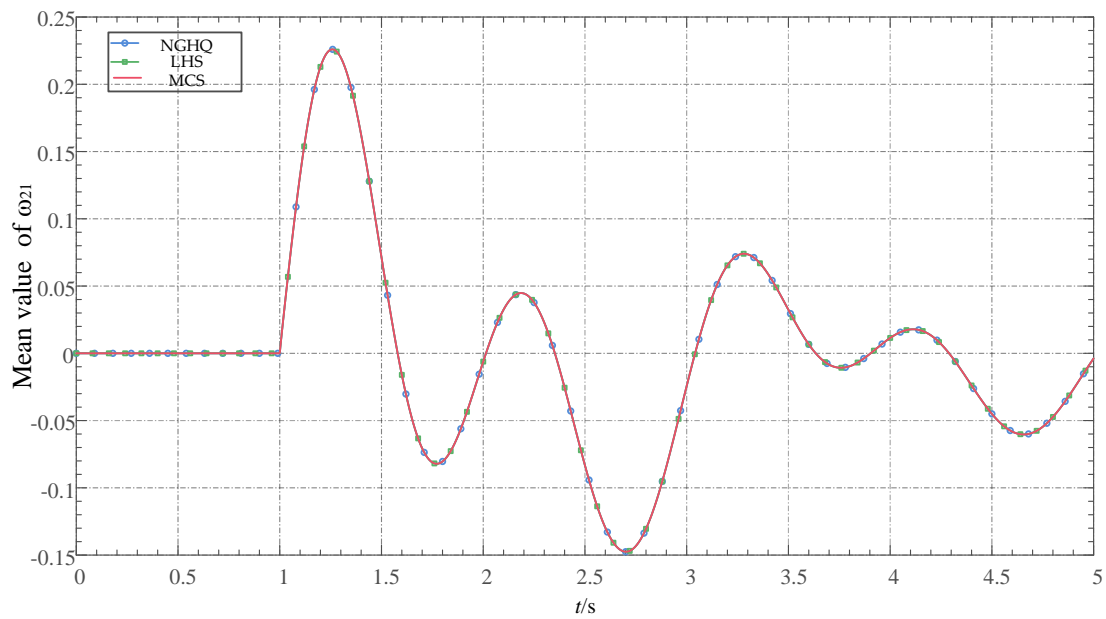


Figure 13. The mean values of ω_{21} about three different methods in the IEEE 39—bus system.

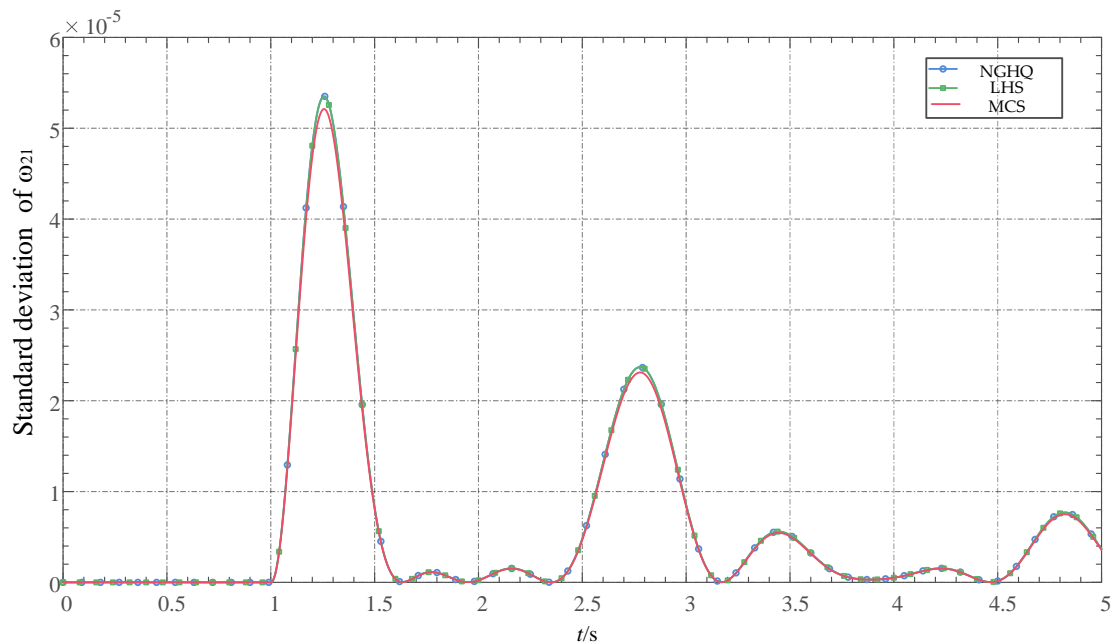


Figure 14. The standard deviations of ω_{21} about three different methods in the IEEE 39—bus system.

From Figures 11–14, it can be seen that the mean values of δ_{21} and ω_{21} calculated by method NGHQ and LHS have little difference with MCS. In addition, the accuracy of the standard deviations of δ_{21} and ω_{21} calculated by NGHQ and LHS is slightly lower than that of MCS, which is negligible in practical engineering applications. It is worth noting that the error always increases at the top and bottom of the peak. The mean and standard deviation of δ_{21} and ω_{21} calculated by NGHQ and LHS are very close. Compared with the IEEE 9—bus system, the standard deviations of δ_{21} and ω_{21} in the IEEE 39—bus system are much smaller, because the dynamic model of the IEEE 39—bus system is more stable. To further verify the effectiveness of the proposed method, Table 4 gives the mean values and standard deviations of each rotation angle at 4 s. It can be seen from Table 4 that the mean values and standard deviations calculated by NGHQ have the same accuracy as those calculated by LHS.

Table 4. Mean values and standard deviations of each rotation angle of different methods at 4 s.

	Mean Values/rad			Standard Deviations/rad ²		
	MCS	LHS	NGHQ	MCS	LHS	NGHQ
δ_1	1.3273	1.3273	1.3273	5.9834×10^{-5}	6.1518×10^{-5}	6.1397×10^{-5}
δ_2	2.0395	2.0395	2.0395	4.0177×10^{-4}	4.1266×10^{-4}	4.1283×10^{-4}
δ_3	1.9673	1.9673	1.9673	1.0033×10^{-4}	1.0307×10^{-4}	1.0297×10^{-4}
δ_4	2.0502	2.0502	2.0502	7.3284×10^{-5}	7.5274×10^{-5}	7.5164×10^{-5}
δ_5	1.9172	1.9172	1.9172	7.5808×10^{-5}	7.7867×10^{-5}	7.7758×10^{-5}
δ_6	1.9540	1.9540	1.9540	7.4994×10^{-5}	7.7030×10^{-5}	7.6920×10^{-5}
δ_7	2.0810	2.0811	2.0811	7.5099×10^{-5}	7.7139×10^{-5}	7.7029×10^{-5}
δ_8	2.0639	2.0639	2.0639	5.7510×10^{-5}	5.9114×10^{-5}	5.8996×10^{-5}
δ_9	2.2011	2.2011	2.2011	6.3321×10^{-5}	6.5059×10^{-5}	6.4950×10^{-5}
δ_{10}	0.8818	0.8818	0.8818	3.1527×10^{-5}	3.2491×10^{-5}	3.2356×10^{-5}

The voltage amplitude of bus 20 is denoted as V_{m20} . Figure 15 shows the mean value of V_{m20} calculated by three different methods. Figure 16 shows the absolute error of the standard deviation of V_{m20} calculated by three different methods. The effectiveness of the proposed method can be verified in Figures 15 and 16. From Figures 15 and 16, it can be seen that the voltage amplitude is much less affected by load uncertainty than the rotation angle and rotation speed. This is because dynamic components such as synchronous generators are the root cause of driving system state changes, and the voltage amplitude changes with the change of system state in order to make the network power balance.

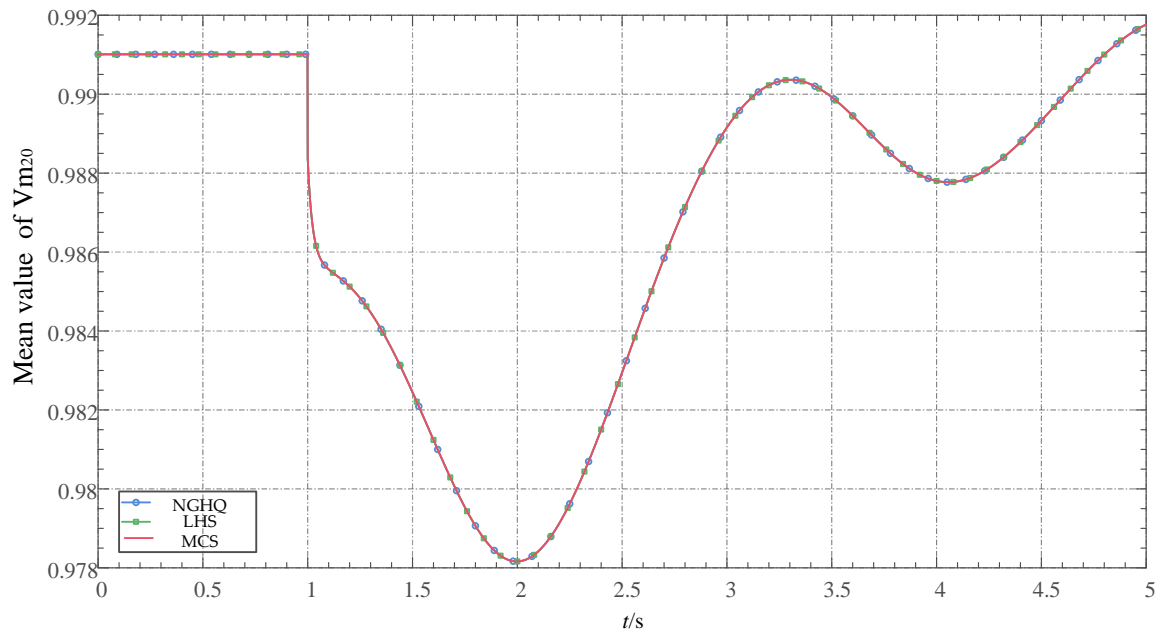
**Figure 15.** The mean values of V_{m20} about three different methods in the IEEE 39—bus system.

Table 5 shows the number of deterministic dynamic simulations N and the total calculation time T in various scenarios. As can be seen from Table 5, compared to MCS and LHS, the proposed method can reduce a large number of dynamic simulation times, thus greatly improving the computational efficiency.

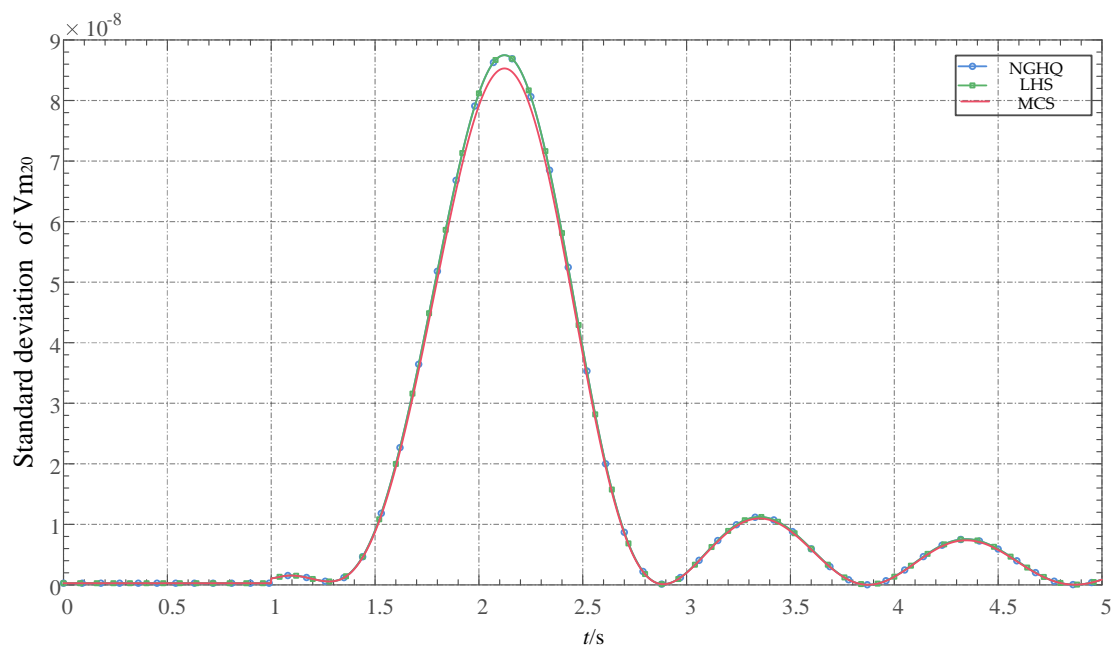


Figure 16. The standard deviations of V_{m20} about three different methods in the IEEE 39—bus system.

Table 5. Simulation times and calculation times of different scenarios in the IEEE 39-bus system.

Scenarios	N	T/s
MCS	20,000	44,011.35
NGHQ – $P = 5$	9	19.94
LHS	1000	2213.18

4. Conclusions

In this paper, a fast power system uncertainty simulation method based on Nataf transformation and Gauss-Hermite quadrature is proposed. Firstly, the sampling samples of input random variables are determined based on Nataf transformation and inverse Nataf transformation. Secondly, the dynamic simulation of power systems is carried out according to the samples. Finally, the mean and standard deviation of state variables and algebraic variables are calculated based on the Gauss-Hermite quadrature.

The simulation results of the IEEE 9-bus system (Appendix A) and IEEE 39-bus system show that compared with the traditional MCS and LHS, the proposed method can obtain accurate mean values of state variables and algebraic variables. Although the standard deviation accuracy is worse than that of the Monte Carlo simulation method, the computational efficiency can be greatly improved. As a non-intrusive method, the proposed method is suitable for complex dynamic models of power systems and can deal with the correlation between input random variables.

Author Contributions: Conceptualization, C.L. and Y.J.; methodology, Y.J.; software, Y.J.; validation, C.L., Y.J., H.B. and R.Y.; formal analysis, C.L. and Y.J.; investigation, L.W. and W.Y.; resources, C.L., H.B., R.Y., L.W. and W.Y.; writing—original draft preparation, Y.J.; writing—review and editing, C.L.; supervision, C.L., Y.J., H.B., R.Y. and L.W.; project administration, H.B., R.Y., L.W. and W.Y. All authors have read and agreed to the published version of the manuscript.

Funding: This research was supported by the National Natural Science Foundation of China under Project 52007133.

Data Availability Statement: All data used to support the findings of this study are included within the article.

Conflicts of Interest: The authors declare no conflict of interest.

Appendix A

Table A1. The static active power (P_{L0}), static reactive power (Q_{L0}), and the static voltage (V_0) of the loads in the IEEE 9-bus system.

Bus	P_{L0} (MW)	Q_{L0} (Mvar)	V_0 (pu)
1	0	0	1.04
2	0	0	1.025
3	0	0	1.025
4	0	0	1.026
5	90	30	1.013
6	0	0	1.032
7	100	35	1.016
8	0	0	1.023
9	125	50	0.996

Table A2. The dynamic parameters of the generators in IEEE 9-bus system.

Generator Number	Bus	D (pu)	R_a (pu)	ω_s (rad/s)	H (pu)	X_d' (pu)
1	1	0.0125	0.0041	120π	23.64	0.0608
2	2	0.0068	0.0026	120π	6.40	0.1198
3	3	0.0048	0.0035	120π	3.01	0.1813

Table A3. Symbol description in the IEEE 9-bus system.

Symbol	Description
D	damping
R_a	internal resistance
ω_s	rated angular velocity
H	inertia
X_d'	d-axis sub-transient reactance

References

1. Wilches-Bernal, F.; Byrne, R.H.; Lian, J. Damping of inter-area oscillations via modulation of aggregated loads. *IEEE Trans. Power Syst.* **2019**, *35*, 2024–2036. [\[CrossRef\]](#)
2. Zheng, C.; Wang, S.; Liu, Y. A novel equivalent model of active distribution networks based on LSTM. *IEEE Trans. Power Syst.* **2019**, *30*, 2611–2624. [\[CrossRef\]](#) [\[PubMed\]](#)
3. Reddy, G.H.; Kiran, M.K.; Kumar, P.S. Fuzzy reliability assessment of distribution system with wind farms and plug-in electric vehicles. *Electr. Power Compon. Syst.* **2019**, *47*, 1791–1804. [\[CrossRef\]](#)
4. Li, J.; Zhang, X.; Zhou, X. Reliability assessment of wind turbine bearing based on the degradation-Hidden-Markov model. *Renew. Energy* **2019**, *132*, 1076–1087. [\[CrossRef\]](#)
5. Lin, Y.; Wang, Y.; Wang, J. Global sensitivity analysis in load modeling via low-rank tensor. *IEEE Trans. Smart Grid* **2020**, *11*, 2737–2740. [\[CrossRef\]](#)
6. Matavalam, A.R.R.; Vaidya, U.; Ajarapu, V. Propagating uncertainty in power system initial conditions using data-driven linear operators. *IEEE Trans. Power Syst.* **2022**, *37*, 4125–4128. [\[CrossRef\]](#)
7. Qiu, Y.; Wu, H.; Song, Y.; Wang, J. Global approximation of static voltage stability region boundaries considering generator reactive power limits. *IEEE Trans. Power Syst.* **2018**, *33*, 5682–5691. [\[CrossRef\]](#)
8. Taghavi, R.; Samet, H.; Seifi, A.R. Stochastic Optimal Power Flow in Hybrid Power System Using Reduced-Discrete Point Estimation Method and Latin Hypercube Sampling. *IEEE Can. J. Electr. Comput.* **2021**, *45*, 63–67. [\[CrossRef\]](#)
9. Li, L.; Qiu, Y.; Wu, H.; Song, Y.; Lei, X. Uncertainty analysis of power system time-domain simulation based on generalized polynomial chaos method. In Proceedings of the 2017 IEEE Power & Energy Society General Meeting, Chicago, IL, USA, 16–20 July 2017.
10. Wang, G.; Xin, H.; Wu, D. Data-driven probabilistic small signal stability analysis for grid-connected PV systems. *Int. J. Electr. Power* **2019**, *113*, 824–831. [\[CrossRef\]](#)
11. Prempraneerach, P.; Hover, F.S.; Triantafyllou, M.S. Uncertainty quantification in simulations of power systems: Multi-element polynomial chaos methods. *Reliab. Eng. Syst. Saf.* **2010**, *95*, 632–646. [\[CrossRef\]](#)

12. Xu, Y.; Mili, L.; Sandu, A. Propagating uncertainty in power system dynamic simulations using polynomial chaos. *IEEE Trans. Power. Syst.* **2018**, *34*, 338–348. [[CrossRef](#)]
13. Wang, X.; Wang, X.; Sheng, H. A data-driven sparse polynomial chaos expansion method to assess probabilistic total transfer capability for power systems with renewables. *IEEE Trans. Power. Syst.* **2020**, *36*, 2573–2583. [[CrossRef](#)]
14. Wang, X.; Liu, R.P.; Wang, X. A data-driven uncertainty quantification method for stochastic economic dispatch. *IEEE Trans. Power. Syst.* **2021**, *37*, 812–815. [[CrossRef](#)]
15. Laowanitwattana, J.; Uatrongjit, S. Probabilistic power flow analysis based on arbitrary polynomial chaos expansion of bus voltage phasor. *Int. Trans. Electr. Energy* **2020**, *30*, e12315. [[CrossRef](#)]
16. Wang, C.; Ma, J.; Shen, Y. Probabilistic load margin assessment considering forecast error of wind power generation. *Energy Rep.* **2023**, *9*, 1014–1021. [[CrossRef](#)]
17. Qiu, Y.; Lin, J.; Chen, X.; Liu, F.; Song, Y. Nonintrusive Uncertainty Quantification of Dynamic Power Systems Subject to Stochastic Excitations. *IEEE Trans. Power. Syst.* **2021**, *36*, 402–414. [[CrossRef](#)]
18. Liu, C.; Wang, B.; Sun, K. Fast power system dynamic simulation using continued fractions. *IEEE Access* **2018**, *6*, 62687–62698. [[CrossRef](#)]
19. Liu, Y.; Sun, K.; Yao, R. Power system time domain simulation using a differential transformation method. *IEEE Trans. Power. Syst.* **2019**, *34*, 3739–3748. [[CrossRef](#)]
20. Lin, X.; Jiang, Y.; Peng, S. An efficient Nataf transformation based probabilistic power flow for high-dimensional correlated uncertainty sources in operation. *Int. J. Electr. Power* **2020**, *116*, 105543. [[CrossRef](#)]
21. Chen, S.; Hu, W.; Du, Y. Three-stage relaxation-weightsum-correction based probabilistic reactive power optimization in the distribution network with multiple wind generators. *Int. J. Electr. Power* **2022**, *141*, 108146. [[CrossRef](#)]
22. Kiureghian, A.; Liu, P. Structural reliability under incomplete probability information. *J. Eng. Mech.* **1986**, *112*, 85–104. [[CrossRef](#)]
23. Jithendranath, J.; Das, D.; Guerrero, J.M. Probabilistic optimal power flow in islanded microgrids with load, wind and solar uncertainties including intermittent generation spatial correlation. *Energy* **2021**, *222*, 119847. [[CrossRef](#)]
24. Liu, Q.; Pierce, D. A note on Gauss–Hermite quadrature. *Biometrika* **1994**, *81*, 624–629.
25. Jin, S.; Andersson, B. A note on the accuracy of adaptive Gauss–Hermite quadrature. *Biometrika* **2020**, *107*, 737–744. [[CrossRef](#)]
26. Zhao, Y.; Ono, T. New point estimates for probability moments. *J. Eng. Mech* **2000**, *126*, 433–436. [[CrossRef](#)]
27. Liu, Y.; Sun, K. Solving power system differential algebraic equations using differential transformation. *IEEE Trans. Power. Syst.* **2019**, *35*, 2289–2299. [[CrossRef](#)]
28. Zimmerman, R.D.; Murillo-Sánchez, C.E.; Thomas, R.J. MATPOWER: Steady-state operations, planning, and analysis tools for power systems research and education. *IEEE Trans. Power. Syst.* **2010**, *26*, 12–19. [[CrossRef](#)]
29. Chen, Y.; Wen, J.; Cheng, S. Probabilistic load flow method based on Nataf transformation and Latin hypercube sampling. *IEEE Trans. Sustain. Energy* **2012**, *4*, 294–301. [[CrossRef](#)]
30. Liu, C.; Qin, N.; Sun, K. Remote voltage control using the holomorphic embedding load flow method. *IEEE Trans. Smart Grid* **2019**, *10*, 6308–6319. [[CrossRef](#)]
31. Wang, B.; Duan, N.; Sun, K. A time-power series-based semi-analytical approach for power system simulation. *IEEE Trans. Power. Syst.* **2018**, *34*, 841–851. [[CrossRef](#)]

Disclaimer/Publisher’s Note: The statements, opinions and data contained in all publications are solely those of the individual author(s) and contributor(s) and not of MDPI and/or the editor(s). MDPI and/or the editor(s) disclaim responsibility for any injury to people or property resulting from any ideas, methods, instructions or products referred to in the content.